Journal of Science and Technology
Engineering and Technology for Sustainable Development
Volume 35, Issue 4, October 2025, 001-008

NO Adsorption on Zeolites and Active Carbon toward the Application for the Treatment of Highly Concentrated NO_x in Industry

Thanh Hung Nguyen[1], Phuong Lien Nguyen[1], Van Duong Le[1], Minh Thang Le[1], Thanh Trung Do[1], Ngoc Toan Vu[2,*]
[1]School of Chemistry and Life Sciences, Hanoi University of Science and Technology, Ha Noi, Vietnam
[2]Institute of New Technology, Ha Noi, Vietnam
[*]Corresponding author email: vntoanchem@gmail.com

Abstract

The development of the economy and industry is accompanied by the emission of a large amount of exhaust gases such as NO, NO_2, and N_2O, which have a negative impact on the environment. In the study, the NO adsorption on zeolites and activated carbon was examined and compared. The absorbents were also characterized using N_2 physical adsorption, NO temperature-programmed desorption, Scanning Electron Microscopy, and Energy-Dispersive Spectroscopy to expose specific surface area, adsorption ability, material morphology, and elemental content of the samples. The results showed that the NO adsorption efficiency on zeolite samples was superior to that of activated carbon due to the larger surface area and higher metal cation content, leading to their higher adsorption capacity due to the chemical adsorption at these metal cation sites. The modification of the adsorbent by adding Fe^{2+} on Zeolite ZX5 has enhanced the active sites that are beneficial for the NO adsorption process, helping to improve the NO adsorption capacity compared to the original sample.

Keywords: activated carbon, adsorption, zeolite, NO, NO_x.

1. Introduction

The era of industrialization and modernization has led to the rapid development of industries and population growth, contributing to economic development. However, along with these benefits, there are environmental consequences, especially air pollution, which harms human health and the living environment of animals and plants. Therefore, the problem of environmental pollution in general and air pollution in particular is one of the urgent global concerns today. Notable effects of NO_x are the formation of acid rain, photochemical smog, ozone depletion, and fog [1, 2].

Recently, research efforts have been continuously carried out to meet the requirements of reducing NO_x emissions with high efficiency in both mobile and stationary sources, in which post combustion treatment methods are widely applied. There are methods for treating NO_x formed after combustion reactions, including adsorption, absorption, desorption, thermal, and chemical treatment. A combination of methods can be used to treat NO_x thoroughly. Alternatively, the methods can be categorized into wet and dry processes based on the reaction environment. The dry method is further subdivided into those that employ a catalyst and those that do not [3]. In the non-catalytic process, the Selective Non-Catalytic Reduction (SNCR) method uses high temperatures (900-1000 ^oC) to reduce NO_x in the presence of a reducing agent such as ammonia (NH_3) or urea ($CO(NH_2)_2$). This method is highly efficient but does not make sense thermodynamically and economically. For the catalytic process, it can be divided into four main directions: (1) Direct NO_x decomposition; (2) Three Way Catalyst - TWC; (3) Selective reduction using hydrocarbon catalyst (HC - SCR); (4) Ammonia Selective Catalytic (NH_3 - SCR) [4, 5].

When the emission sources possess not too high NO_x concentrations, such as the exhaust gases from vehicles and thermal power plants…, the NO_x treatment method by selective non-catalytic reduction (SNCR) or selective catalytic reduction (SCR) with NH_3 is still the optimal choice due to its high efficiency and reasonable cost. However, for factories with high NO_x emissions, such as chemical fertilizer and explosives factories, selective catalytic reduction (SCR) will not be highly effective, causing a waste of NO_x resources. Therefore, the adsorption method can be applied. The amount of adsorbed NO_x can be recovered by the desorption at high temperatures afterward. The high recovered NO_x concentration could be used for the nitric acid production process to serve many different needs in the industry. The adsorption process is carried out on an adsorption system using solid adsorbents. Exhaust fans collect the exhaust gas from the factory, which is then pushed by the fan system into the absorption columns with solid adsorbent materials. The adsorbed gas is then

p-ISSN 3093-3242
e-ISSN 3093-3579
https://doi.org/10.51316/jst.185.etsd.2025.35.4.1
Received: Dec 16, 2024; revised: Feb 10, 2025
accepted: Apr 8, 2025; Online: Sep 20, 2025.

desorbed by raising the temperature and using an inert gas flow to separate it from the adsorbent.

Solid materials selected as adsorbents must have outstanding characteristics such as a large specific surface area, capillaries suitable for the adsorbed substance, selective adsorption capacity, and easy desorption and reuse. Typical materials include activated carbon, zeolite, and MOF (Metal-organic Frameworks). Activated carbon is often activated under high temperatures in an anaerobic environment to create a porous structure, increasing the contact surface area for adsorption or chemical reactions [6]. In the study of Mei-Ling Fang *et al*. (2019), a mechanism for NO_2 adsorption onto activated carbon was proposed [7]: NO_2 can be directly adsorbed/desorbed by the "-C*" functional group, forming an unstable -C(ONO) that tends to decompose and release a NO molecule and form a -C(O) group. The -C(O) functional group can bond with two NO_2 and temporarily form two -2C(ONO_2) groups. Next, the C(ONO_2) groups can react with the excess NO_2 molecule and form a more stable functional group -C(ONO_3). On the other hand, two adjacent -C(NO_2) groups can be combined and converted to a stable -C_2(ONO_2), and a NO molecule will escape from the AC surface. Finally, C_2(ONO_2) can be decomposed and form -C(O) and NO when the carbon is thermally regenerated. Here we use -C* for active site on the carbon surface, and -C(O) for oxygenated carbon surface.

Therefore, zeolites have high adsorption and selectivity properties. Molecules that are significantly bigger than the pore size are pushed out and not adsorbed on zeolites [8, 9]. Zeolites are formed based on the basic MO_4 structural units of silica tetrahedra $[SiO_4]^{4-}$ and alumina tetrahedra $[AlO_4]^{5-}$ linked together through common oxygen vertices. The primary structural units are the same in all types of zeolites (The center is silicon or aluminum, and the vertex is oxygen). Each tetrahedron is linked to the remaining tetrahedrons through the oxygen atom at the vertex of each tetrahedron, forming -Si-O-Si or -Si-O-Al- bonds [10]. In the study of E. P. Hessou and colleagues (2018), an adsorption mechanism based on ion exchange interactions between NO_x molecules and zeolite was proposed. NO is adsorbed through the primary interaction shown by the compensating cation Mn^+ bonded to nitrogen atoms. The interaction energy between NO and a proton in this zeolite structure is about -25 kJ/mol [7]. The NO_2 molecule has the exact mechanism as NO, adsorbing through nitrogen and a secondary interaction created by one of the two oxygen atoms with an energy level of -30 kJ/mol.

In this work, we aimed to compare the NO adsorption capacity of zeolite samples with that of the activated carbon sample. In addition, the pore size of the materials was determined by N_2 physical adsorption methods to evaluate their effects on the adsorption capacity. To improve the adsorption performance of zeolites, Fe^{2+}, which is considered to have good NO adsorption affinity in many studies [10], has been impregnated on zeolites.

2. Experiment

2.1. Materials

Zeolites were prepared previously in the laboratory. Different samples with the main composition of zeolite 13X mixed with different binders (boehmite or silica gel and other minor binders) to form different pellet shapes are symbolized as ZX5, 13X, ZX31 and ZX6. Activated carbon (AC) in pellet form was commercially purchased in Vietnam. Pictures of the samples are shown in Fig. 1.

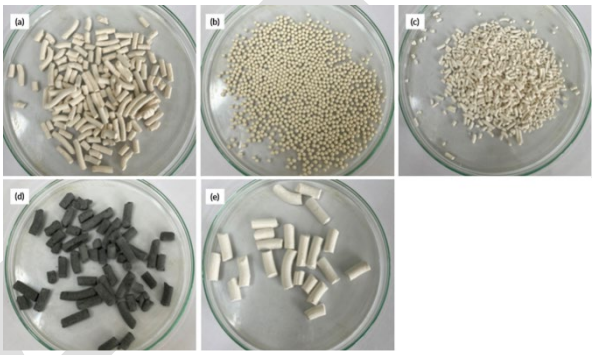

Fig. 1. Original shape of adsorbent materials: a) Zeolite ZX5 (zeolite 13X+ 15% boehmite, pellets, 4 mm diameter, 0.6 - 1.2 cm length, calcination temperature: 610 ºC); b) Zeolite 13X (zeolite 13X, sphere, 2 mm diameter, calcination temperature 400 ºC); c) Zeolite ZX31 (zeolite 13X + 25% boehmite, pillars, 2 mm diameter, 0.25 - 0.6 cm length, calcination temperature 550 ºC); d) Activated carbon (pellets, 5 mm diameter, 0.7 - 1.2 cm length); e) Zeolite ZX6 (zeolite 13X + 15% silica gel, pellets, 6mm diameter, 0.9 - 2 cm length, calcination temperature: 610 ºC)

Preparation of Fe^{2+} impregnation sample on ZX5 (ZX5.Fe^{2+}): Apparently, 0.2744 g of $FeSO_4.7H_2O$ was dissolved in 50 mL of distilled water for 15 minutes. Then, 2.5 g of ZX5 was added to the above solution and stirred with a magnetic stirrer at 65-70 °C for 12 hours. This impregnation process was carried out under two conditions: maintaining stirring in an air environment or a flow of N_2 gas through the system. The sample was dried overnight (about 12 hours) at 90-100 °C in an air environment or a flow of N_2 gas. The composite samples in Air and N_2 were denoted Air/ZX5.Fe^{2+}; N_2/ZX5.Fe^{2+}, respectively.

2.2. Characterization of the Materials

Emission Scanning Electron Microscope (SEM), Elemental mapping, and Energy-Dispersive Spectroscopy (EDS) measurement were performed on a JEOL JCM-7000 (Japan) integrated with an X-ray energy dispersive spectrometer (EDS) at the GeViCat Center, Hanoi University of Science and Technology. NO temperature programmed desorption (NO- TPD) was measured as follows: 0.15 (g) of a sample was put

directly into the analysis tube, which was then placed in the measuring device. First, the sample was pretreated by introducing an inert Helium gas flow at a rate of 30 mL/min from room temperature to 300 °C, the heating rate of 3 °C/min, and holding for 30 minutes to remove water and volatile substances in the sample. Then, the sample was cooled to 50 °C. After the sample had been surface cleaned and the sample temperature cooled to 50 °C, then 5% NO/He flow with a flow rate of 30 mL/min was introduced into the sample tube to carry out the NO adsorption process for 60 minutes. The samples were heated in a He gas stream at a 30 mL/min flow rate from 50 to 600 °C at a heating rate of 10 °C/min and held at 600 °C for 30 min. The gas stream from the device was passed through a mass spectrometer. The samples were measured on an AutoChem II 2920 V5.02 combined with a Cirrus 2-MKS spectrometer at the GeViCat Center, Hanoi University of Science and Technology. The N_2 adsorption-desorption (BET) method determined the materials' specific surface area. This method was performed on a Micromeritics Gemini VII 2390 (USA). The sample was vacuum treated at 150 °C for 1 hour and increased to 300 °C for 1 hour before measurement. The sample was then cooled to room temperature, pressure equilibrated with 99.999% N_2, and weighed to re-determine the sample mass. The sample was introduced into the N_2 adsorption apparatus at -196 °C (77 K), with an N_2 gas flow rate of 25 mL/min.

2.3. Measurement of Adsorption Capacity

The sample was tested according to the scheme in Fig. 2. The initial sample was pretreated to remove water vapor and absorbed gases in the sample. Briefly, about 0.25 grams of adsorbent material was put it into the reaction column fixed by glass wool. Then, the sample was heated to 150 °C at a rate of 5 °C/min. Simultaneously, a 99.999% Ar was purged at a flow rate of 60 mL/min through the tube containing the adsorbent material to remove unwanted impurities in the material and maintain the system's temperature at 150 °C for 1 hour. After that, it was cooled down to room temperature.

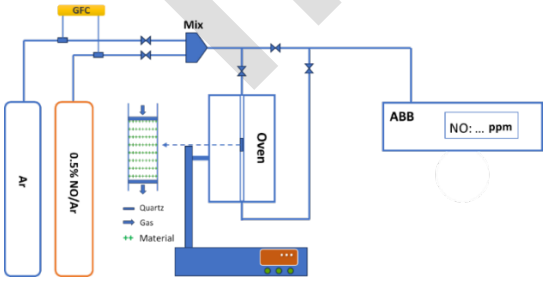

Fig. 2. Diagram of NO gas adsorption and desorption system

Adsorption process: 0.5% NO/Ar gas mixture was purged through the tube containing the treated material at a flow rate of 20.5 mL/min. The output gas (NO) was detected by a UV-multi-gas sensor detector (ABB gas Analyzer models AO-2020, Limas 21HW, Mannheim, Germany), and the concentration values were displayed and recorded every 15 seconds until the gas concentration did not change.

Desorption process: the tested sample was heated to 200 °C at a rate of 5 °C/min under Ar flow at a 20.5 mL/min. The output gas (NO) was detected by a UV-multi-gas sensor detector (ABB gas Analyzer models AO-2020, Limas 21HW, Mannheim, Germany). NO concentration is measured and recorded every 15 seconds until the gas concentration does not change.

Adsorbed Quantity (A_{ads}) was calculated as:

$$A_{ads} = \frac{Q_{out} \times S_{ads} \times 10^{-6}}{22{,}4 \times m}, \text{mmol/g} \quad (1)$$

$$S_{ads} = \sum_0^t \left[\frac{1}{2} \times \left(2C_{max} - (C_i + C_{i+1})\right) \times \Delta t\right] \quad (2)$$

Desorbed Quantity (A_{des}) was calculated as:

$$A_{des} = \frac{Q_{out} \times S_{des} \times 10^{-6}}{22{,}4 \times m}, \text{mmol/g} \quad (3)$$

$$S_{des} = \sum_0^t \left[\frac{1}{2} \times \left(C_j + C_{j+1} - 2C_{min}\right) \times \Delta t\right] \quad (4)$$

where:

Q_{out}	Flow rate (mL/min) of the 0.5% NO/Ar flow in the adsorption process and the Ar flow in the desorption process
S_{ads}	Area formed by the vertical axis, horizontal axis, and adsorption process graph in adsorption process (ppm.min)
S_{des}	Area formed by the vertical axis, horizontal axis, and desorption process graph in desorption process (ppm. min)
C_{max}	Initial NO concentration (ppm)
C_{min}	Final NO concentration of measurement (ppm)
C_i	NO concentration at time *i* in the adsorption process (ppm)
C_j	NO concentration at time *j* in the desorption process (ppm)
Δt	Time between 2 measurements (minutes)
m	Mass of catalyst (grams)

3. Results and Discussion

SEM images of adsorbents are presented in Fig. 3. The images show that the surface of the samples is uneven, in which the granular structures are interconnected to form large structures. These granular structures have heterogeneous sizes, shapes, and distributions. The 13X surface is smoother than the other samples, while the activated carbon (AC) sample shows a sizeable porous surface. The 13X sample also has smaller particles distributed on the surface. The ZX5 sample before and after Fe^{2+} impregnation (N_2/ZX5.Fe^{2+}) does not have much change in shape and surface structure.

EPR spectrum for sample ZX5.Fe^{2+} was synthesized under two conditions, Air and N_2, denoted as Air/ZX5.Fe^{2+} and N_2/ZX5.Fe^{2+} was measured at room temperature in the measuring range 500 - 2500 G. A signal appears at B = 1570 G. Substituting B into formula (5), the g factor can be calculated:

$$g = 0.7145 \times \frac{\nu}{B} = 0.7145 \times \frac{9400}{1570} = 4.28 \quad (5)$$

where:

g	the electron's so-called g-factor
v	microwave frequency (GHz)
B	Magnetic field (Gauss)

The signal peak at g (=) equal to 4.28 is assigned to isolated Fe^{3+} ions located in octahedral/tetrahedral coordination sites with strong rhombohedral distortion, which have resonance lines at g (≈) approximately to 4.26 and g (≈) equal approximately to 2.0 [11]. Meanwhile, Fe^{2+} salt does not show a signal on EPR because it is a diamagnetic ion [12]. The Fe^{2+}-impregnated ZX5 sample synthesized in air conditions (Air/ZX5.Fe^{2+}) shows a significant intensity peak at this position, indicating that there was a transformation from Fe^{2+} salt to Fe^{3+} during the synthesis process. At the same time, the Fe^{2+}-impregnated ZX5 sample synthesized in N_2 conditions shows a much lower intensity peak than that of the above sample. Here, the synthesis in the absence of O_2 helped to prevent the formation of Fe^{3+} better. Therefore, the sample synthesized under N_2 conditions was chosen as the NO adsorbent.

Elemental mapping was applied to the zeolite samples to evaluate the elements' distribution on the material surface. The results in Fig. 4 show that the elements O, K, Na, Si, and Al, which are the main constituents of ZX5, were evenly distributed on the sample surface and in the shape of the grain structures. After impregnation with Fe^{2+}, the results showed that the appearance of the Fe element was evenly distributed on the surface. This result showed that the impregnation process successfully brought Fe to the ZX5 surface.

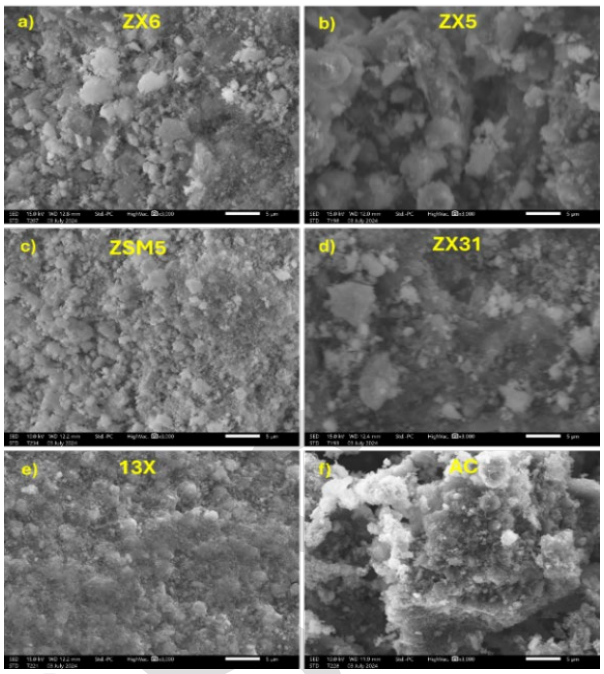

Fig. 3. SEM images of materials with different magnifications of 3000x a) ZX6; b) ZX5; c) N_2/ZX5.Fe^{2+}; d) ZX31; e) 13X; f) AC

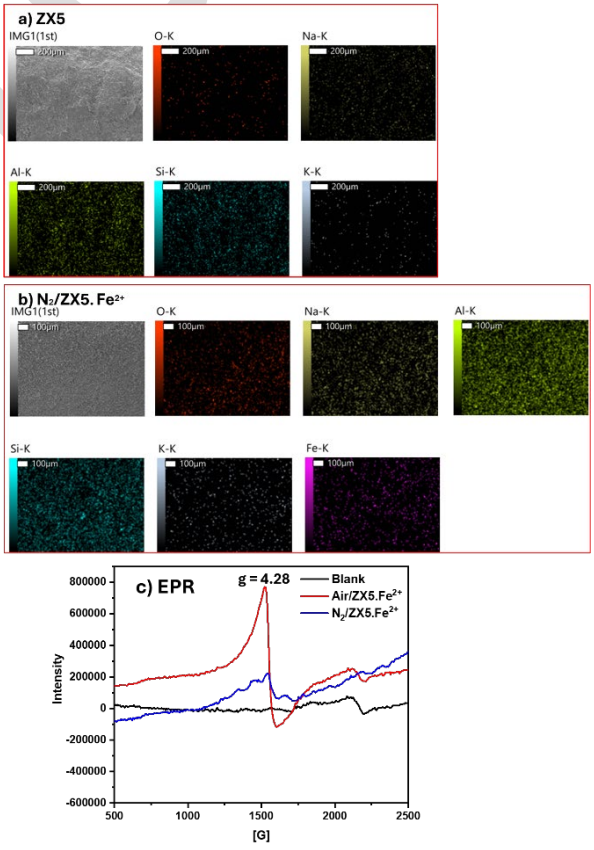

Fig. 4. Elemental mapping graphs of a) ZX5 and b) N_2/ZX5.Fe^{2+}, c) EPR of samples

Table 1. Element composition (from EDS) and surface area of the samples

Sample	Weight %	% Atom						Ratio Si/Al	S_{BET} (m^2/g)
	Fe	O	Si	Al	Na	K	Fe		
ZX6	0	55.6	15.2	18.5	9.9	-	-	0.8	60.8
13X	0	61.7	15.3	11.7	10.2	1.1	-	1.3	10.5
ZX31	0	54.8	12.6	27.3	6.8	0.3	-	0.3	150.7
ZX5	0	58.4	13.1	21.0	7.5	-	-	0.6	61.9
N_2/ZX5.Fe^{2+}	5.5	55.9	15.0	20.3	6.0	-	2.2	0.7	176.9
AC	0	-	-	-	-	-	-	-	18.0

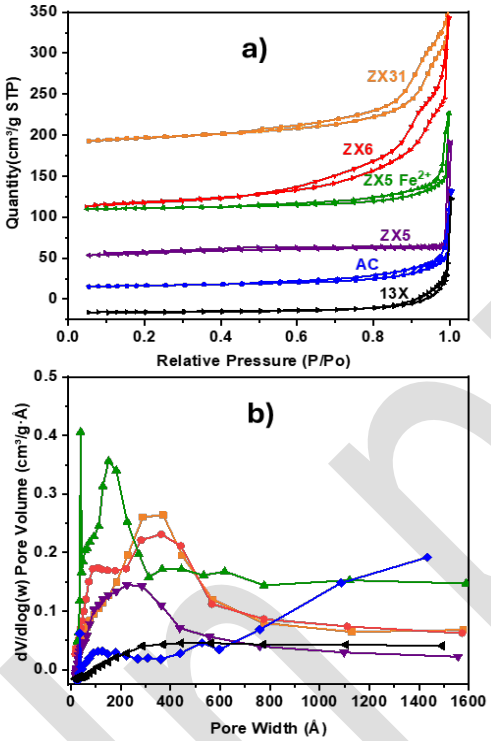

Fig. 5. a) N_2 adsorption/desorption isotherms and b) Pore size distribution

According to the Energy-Dispersive Spectroscopy (EDS) results from Table 1, the mass ratio of Fe impregnated on the ZX5 (N_2/ZX5.Fe^{2+}) sample is approximately the same as the theory. This shows that the previous impregnation process has achieved the desired ratio. The zeolite material samples have Si/Al ratios ranging from 0.3 - 1.30. ZX31 contains the highest Al content, which can be more acidic [13, 15]. Zeolites have TO_4 tetrahedra (SiO_4 or AlO_4^-) linked by oxygen atoms to form the main structures; however, the presence of AlO_4^- creates a negative charge in the structure and needs to be neutralized by exchangeable compensating cations (e.g., Na^+, K^+, Ca^{2+}). These cations are known to be able to change some properties of zeolite, especially for adsorption processes [16].

The N_2 adsorption-desorption isotherms and the pore distribution of the adsorbent material samples are shown in Fig. 5. Since the analysis system is limited to determining the average pore size and above, only the pore distribution from the average pore size and above is considered in this measurement. The results show that all materials exhibit type IV isotherms, which are typical of medium-pore materials (20 Å < d < 500 Å) [17].

From the shape of the hysteresis loop observed with the H_2 type hysteresis loop (0.6< P/Po< 1) with the pore size concentrated at 200 Å and 500 Å, it shows that the material contains diverse types of pores and the pore diameter distribution is relatively large, with the capillaries having a bottleneck shape, narrow at the top and large at the bottom recorded on the samples: ZX31; ZX6; ZX5 and N_2/ZX5.Fe^{2+}. For AC, the hysteresis loop is narrower, belonging to the H_3 type (0.45< P/P_o< 1), which is typical for capillaries with a slit shape with uneven size and mainly concentrated in the range of 50-300 Å [17, 18]. In addition, there is the appearance of large capillary pores (>800 Å), possibly due to the adhesion of AC unit particles to these sites. Normally, powdered zeolites and powdered activated carbon (AC powder) have quite large specific surfaces. However, in this study, materials were pelletized with larger sizes, leading to a large decrease in specific surface area, as seen in Table 1. However, N_2/ZX5.Fe^{2+} possesses a significantly increased surface area compared to the original ZX5 sample. ZX5 sample has low mechanical strength, therefore during the impregnation of Fe^{2+}, the sample surface was broken partly due to the stirring in an aqueous solution at 70 °C, and the partial dissolution of the binders and surface particles occurred, resulting in the decrease of particle size and the loosening of surface particles, thus leading to a significant increase in surface area, closer to the surface area of original zeolite (before making to the pellets). Besides, when Fe^{2+} is impregnated on the ZX5 sample, no significant changes in capillary size and properties were recorded. In addition, the NO molecule size is only about 1.12 Å [19], so the used materials can fully adsorb NO.

Table 2. NO adsorption quantity was measured by the NO-TPD of the materials

Sample	Temperature at Maximum (°C)	NO adsorption quantity (mmol/g)	Total quantity (mmol/g)
ZX31	81	1.01	10.62
	436	9.61	
ZX5	83	2.05	7.54
	330	5.49	
N_2/ ZX5.Fe^{2+}	82	2.02	8.25
	300		
	433	6.23	

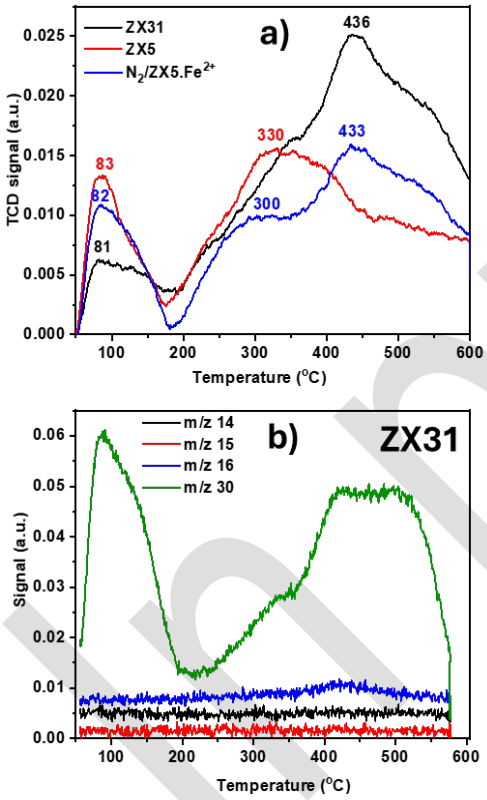

Fig. 6. a) NO-TPD profiles of ZX31; ZX5; N_2/ZX5.Fe^{2+} and b) Signal mass of ZX31

NO-TPD was performed on samples with large specific surfaces ZX31, ZX5, and N_2/ZX5.Fe^{2+}. The results shown in Fig. 6 a) and Table 2 show two NO desorption regions above and below 300 °C. The peaks below 300 °C are attributed to weak physical and chemical adsorption sites on the surface. The results show that all samples have small adsorption peaks at around 80-85 °C, in which the NO desorption capacity of the samples indicates that ZX31 exhibits the lowest value, whereas N_2/ZX5.Fe^{2+} and ZX5 present nearly identical capacities. With the temperature range above 300 °C, the peaks are attributed to chemical adsorption sites formed by the thermal decomposition of nitrate and/or nitrite species generated by NO adsorption on the material, thanks to the ion exchange capacity at each AlO_4 tetrahedron in the zeolite framework. The adsorption mechanism based on the ion exchange interaction between NO_x molecules and zeolites was proposed by E. P. Hessou *et al.* (2018) [7]. The results show that NO was absorbed on ZX5 at the lowest temperature (330 °C) and the smallest capacity among the analyzed samples.

Sample N_2/ZX5.Fe^{2+} desorbed NO at two peaks, 300 and 433 °C, the total desorption capacity was larger than that of ZX5, which showed that the presence of Fe^{2+} improved the chemical adsorption capacity for ZX5. Besides, ZX31 also had a peak at 436 °C with the largest desorption capacity compared to the remaining samples, which could be due to the superior specific surface area leading to large adsorption centers and the ability of NO to contact those sites. In addition, the smallest Si/Al ratio of 0.31 showed that a large amount of Al led to a large enhancement of the active sites of the sample. In the study of L. Beco *et al.*, the multiple adsorptions of NO on Fe^{2+} cations of Ferrierite were proposed. When a single NO molecule is adsorbed, a tetragonal pyramid is formed with four Fe-O bonds in the plane with the framework and one axial Fe-N bond. A cis tetrahedral complex is formed when a second NO molecule is adsorbed on the Fe^{2+} cation. The tetrahedral complex contains a $[Fe\text{-}(NO)_2]^+$ (dinitrosyl) particle, which carries only a single positive charge. Since such a particle compensates for only one Al/Si substitution, the resulting charge imbalance causes a high chemical reactivity of the Al framework sites. Therefore, a third NO molecule absorbs the activated oxygen atoms adjacent to the Al site [20].

Combined with the NO-TPD analysis of the ZX31 sample, the mass spectra of the desorbed gas flow were also recorded, which showed masses 14, 15, 16, and 30 m/z corresponding to N, O, and NO molecules. Fig. 6 b) shows that the significant increase in signal intensity only appears for the mass 30 m/z corresponding to NO at two different temperature regions, which is consistent with the NO-TPD results, proving that during the NO desorption process, only NO is released. The existence of NO chemical adsorption centers on the surface leads to the fact that NO is difficult to release and requires higher desorption temperatures.

Table 3. NO adsorption and desorption quantity measured by NO adsorption-desorption experiments in the microreactor setup

Sample	Quantity NO adsorption (mmol/g)	Quantity NO desorption (mmol/g)	% Retained NO
AC	0.052	0.014	73.07
13X	0.117	0.015	87.17
ZX5	0.234	0.010	92.72
ZX6	0.350	0.014	93.00
ZX31	1.130	0.017	99.50

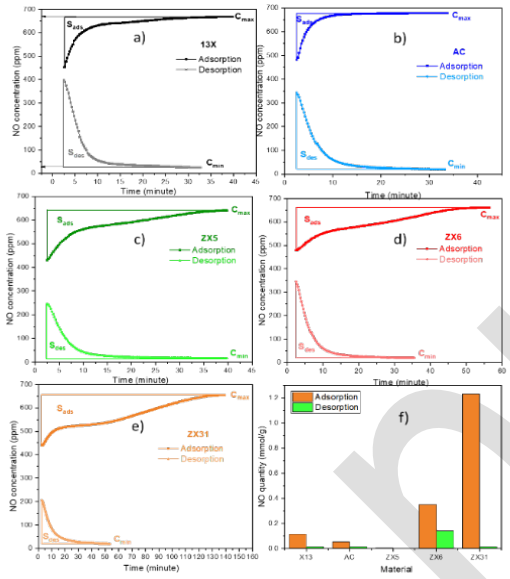

Fig. 7. NO adsorption and desorption curves of materials

The adsorption ability of all samples was also measured by using an adsorption experiment in a microreactor set, as shown in Fig. 2. The results are summarized in Fig. 7 and Table 3. The results show that the adsorption amount of the samples increases gradually, with AC exhibiting the lowest value, followed by 13X, ZX5, and ZX6, and reaching the highest in ZX31, which attained an adsorption capacity of 1.13 mmol/g. However, the desorption capacity of the samples at 200 ºC was much smaller, accounting for only 1.5-27 % of the adsorption amount, showing that the absorbents adsorbed NO tightly and hardly released NO at low desorption temperatures. On the contrary, ZX5 has a lower adsorption ability than ZX31 but has a better desorption ability. This leads to the better reuse ability for NO adsorption processes of ZX5. Moreover, the results of the TPD-NO analysis without a physical adsorption removal stage showed that ZX5 has a better physical adsorption capacity than ZX31, while ZX31 has a better chemical adsorption capacity. Therefore, in this study, Fe^{2+} was impregnated on ZX5 instead of ZX31 to enhance the adsorption capacity, especially the chemical adsorption sites for the sample to a reasonable level (not too weak, not too strong).

Amongst the samples investigated, AC has low NO adsorption capacity but gives higher NO desorption efficiency than the others due to possessing a much lower surface area and bigger pore size. In particular, the existence of large capillary pores facilitates the easy release of NO molecules. In contrast, zeolite samples possess pores concentrated on smaller sizes (10-40nm), which is more suitable for the NO molecular size. Therefore, NO can adsorb easier. The NO release process also becomes more difficult due to the small pore size structure, making it difficult for NO gases to exit. Moreover, the existence of metal sites in zeolite may form the stable NO chemical adsorption

4. Conclusion

In summary, the NO adsorption ability of the investigated samples increased progressively from AC, through 13X, ZX5, and ZX6, to the highest in ZX31. The zeolite samples have better adsorption capacity than activated carbon. Zeolite has a larger surface area and higher cation content, so it has a higher adsorption capacity due to the chemical adsorption on these sites. Zeolite ZX31 has the strongest adsorption capacity (1.13 mmol/g) among the investigated materials, but the affinity with NO is rather high, so the desorption ability at low temperatures (200 ºC) is very small, leading to the difficulty to reuse. The modification of zeolite ZX5 with Fe^{2+} has further enhanced the active sites that are beneficial for NO adsorption of ZX5, helping to improve the NO adsorption capacity compared to the original sample.

Acknowledgments

This research has been supported by Project "Research on identifying cleaner production processes to Control and minimize environmental pollution risks for chemical-explosive materials factories in the military" (Code: 2023.85.54). The authors acknowledge the facilities, the scientific and technical assistance at GeViCat Laboratory/Hanoi University of Science and Technology, established by the Rohan Project funded by the German Academic Exchange Service (DAAD, No. 57315854) and the Federal Ministry for Economic Cooperation and Development (BMZ) inside the framework "SDG Bilateral Graduate school program".

References

[1] Tuan Doan, Anh Dang, Dat Nguyen, Thanh Huyen Vuong, Minh Thang Le, and Huyen Pham Thanh, Hybrid Cu-Fe/ZSM-5 catalyst prepared by liquid ion-exchange for NO_x removal by NH_3-SCR process, Journal of Chemistry, vol. 2021, iss. 1, Jun. 2021. https://doi.org/10.1155/2021/5552187

[2] WANG, Zixian, Air quality analysis of nitrogen oxides and relationships with ozone pollution, PhD Thesis, Kansas State University, 2020.

[3] Rosenberg, H. S., Curran L. M., Slack, A. V., Ando, J., Oxley, J. H., Post combustion methods for control of NOx emissions, Progress in Energy and Combustion Science, vol. 6, iss. 3, pp. 287-302, 1980. https://doi.org/10.1016/0360-1285(80)90020-9

[4] Granger, Pascal, and Vasile I. Parvulescu, Catalytic NOx abatement systems for mobile sources: from three-way to lean burn after-treatment technologies, Chemical Reviews, vol. 111, iss.5, pp. 3155-3207, Mar. 2011. https://doi.org/10.1021/cr100168g

[5] Minghui Zhu, Jun-Kun Lai, Uma Tumuluri, Michael E. Ford, Zili Wu, and Israel E. Wachs, Reaction pathways and kinetics for selective catalytic reduction (SCR) of acidic NO_x emissions from power plants with NH_3, ACS Catalysis, vol. 7, iss. 12, pp. 8358-8361, Dec. 2017. https://doi.org/10.1021/acscatal.7b03149

[6] Bartosz Gurzęda, Nicolas Boulanger, Laura-Bianca Enache, Marius Enachescu, and Aleksandr V. Talyzin, Microporous hydrophilic super-oxidized carbons with high surface area for removal of copper ions, Microporous and Mesoporous Materials, vol. 378, Oct. 2024. https://doi.org/10.1016/j.micromeso.2024.113259

[7] Mei-Ling Fang, Ming-Shean Chou, Cheng-Yu Chang, Hsiao-Yu Chang, Chih-Hsiang Chen, Sheng-Lun Lin, and Yen-Kung Hsieh, Chemical adsorption of nitrogen dioxide with an activated carbon adsorption system, Aerosol and Air Quality Research, vol. 19, iss. 11, pp. 2568-2575, Nov. 2019. https://doi.org/10.4209/aaqr.2019.09.0439

[8] Veena Sodha, Rama Gaur, Rajib Bandyopadhyay, and Syed Shahabuddin, Zeolite-based nanocomposites for wastewater treatment, Tailored Functional Materials: Select Proceedings of MMETFP 2021, Singapore: Springer Nature Singapore, pp. 295-306, 2022. https://doi.org/10.1007/978-981-19-2572-6_23

[9] Pérez-Botella, Eduardo, Susana Valencia, and Fernando Rey. "Zeolites in adsorption processes: State of the art and future prospects, Chemical reviews, 122.24, 17647-17695, 2022. https://doi.org/10.1021/acs.chemrev.2c00140

[10] Feng-Shou Xiao, and Xiangju Meng, Zeolites in sustainable chemistry, zeolites in sustainable chemistry: Synthesis, characterization and catalytic applications, Springer, 2016. https://doi.org/10.1007/978-3-662-47395-5

[11] Jelena Korać, Dalibor M. Stanković, Marina Stanić, Danica Bajuk-Bogdanović, Milan Žižić, Jelena Bogdanović Pristov, Sanja Grgurić-Šipka, Ana Popović-Bijelić, and Ivan Spasojević, Coordinate and redox interactions of epinephrine with ferric and ferrous iron at physiological pH, Scientific Reports, vol. 8, Feb. 2018. https://doi.org/10.1038/s41598-018-21940-7

[12] Y. Guerra, L. Leal, M. Cabrera-Baez; E. Padrón-Hernández, S. Castro-Lopes, Bartolomeu C. Viana, G. Abreu, J. Caland, P. Matos-Rodrigues, F. Santos, J. Matilla-Arias, and R. Peña-Garcia, Cation distribution, Fe^{2+}/Fe^{3+} valence states and oxygen vacancies detection in the $Y_{2.98}Er_{0.02}Fe_5$-yCryO_{12} compound, Journal of Alloys and Compounds, vol. 960, Oct. 2023. https://doi.org/10.1016/j.jallcom.2023.170607

[13] Feng Gao, Nancy M. Washton, Y. Wang, M. Kollár, J. Szanyi, and C. H. F. Peden, Effects of Si/Al ratio on Cu/SSZ-13 NH_3-SCR catalysts: implications for the active Cu species and the roles of Brønsted acidity, Journal of Catalysis, vol. 331, pp. 25-38, Nov. 2015. https://doi.org/10.1016/j.jcat.2015.08.004

[14] Marakatti, Vijaykumar S., and Eric M. Gaigneaux, Alkylation of resorcinol with tertiary butanol over zeolite catalysts: Shape selectivity vs acidity, Catalysis Communications, vol.152, Apr. 2021. https://doi.org/10.1016/j.catcom.2021.106291

[15] Tao Meng, Dongsen Mao, Qiangsheng Guo, and Zhen Ma, Effect of the Si/Al ratios of nanocrystalline HZSM-5 zeolite on the performance in catalytic conversion of ethanol to propylene, Journal of Nanoscience and Nanotechnology, vol. 17, iss. 6, pp. 3779-3785, Jun. 2017. https://doi.org/10.1166/jnn.2017.13992

[16] M. C. Bacariza, R. Bértolo, I. Graça, J. M. Lopes, and C. Henriques, The effect of the compensating cation on the catalytic performances of Ni/USY zeolites towards CO_2 methanation, Journal of CO_2 Utilization, vol. 21, pp. 280-291, Nov. 2017. https://doi.org/10.1016/j.jcou.2017.07.020

[17] Christian Blaker, Johanna Muthmann, Christoph Pasel, Dieter Bathen, Characterization of Activated Carbon Adsorbents- State of the Art and Novel Approaches, ChemBioEng Rev, vol. 6, iss. 4, pp. 119-138, July. 2019. https://doi.org/ 10.1002/cben.201900008

[18] Longfei Xu, Jinchuan Zhang, Jianghui Ding, Tong Liu, Gang Shi, Xingqi Li, Wei Dang, Yishan Cheng, and Ruibo Guo, Pore structure and fractal characteristics of different shale lithofacies in the long formation in the western area of the lower yangtze platform, Minerals, vol. 10, iss. 1, Jan. 2020. https://doi.org/10.3390/min10010072

[19] Greenwood, Norman Neill, and Alan Earnshaw, Chemistry of the Elements. Elsevier, 2012.

[20] L. Benco, T. Bučko, R. Grybos, Jürgen Hafner, Zdeněk Sobalík, Jiří Dědeček, Štěpán Sklenák, and Jan Hrušák, Multiple adsorption of NO on Fe^{2+} cations in the α-and β-positions of ferrierite: an experimental and density functional study, The Journal of Physical Chemistry C, vol. 111, pp. 9393-9402, 2007. https://doi.org/10.1021/jp0724018